

Structural Optimization and Material Fitting of a Material with Inherent Bistable Elements

Zuzana Dimitrovová^{1,3}, Jan Heczko², Libor Lobovský², Jan Krystek², Helder C. Rodrigues³

¹Departamento de Engenharia Civil, Faculdade de Ciências e Tecnologia, Universidade Nova de Lisboa, Lisboa, Portugal
zdim@fct.unl.pt

²NTIS - New Technologies for the Information Society, Faculty of Applied Sciences, University of West Bohemia, Plzeň, Czech Republic

{jheczko, lobo, krystek}@kme.zcu.cz

³IDMEC, Instituto Superior Técnico, Universidade de Lisboa, Lisboa, Portugal
hcr@tecnico.ulisboa.pt

1. Abstract

This paper is focused on material realization and numerical assessment of a negative stiffness phase. The new idea is formulated as to build such a phase by polyethylene foam of low density with special cuts to create a Structure with inherent, periodically distributed, bistable elements (SIBE). SIBE results under displacement control tests verified that the attained global loss factor is much higher than the one of the base material (BM). Therefore it is expected that significant improvements could be obtained if sizes, shapes and arrangements of the additional cuts would be subjected to techniques of structural and design optimization. With this objective convenient material model is defined, its parameters are fitted and optimized according to experiments and finite element model capable of reproducing experimental tests is developed.

2. Keywords: Negative stiffness, Material fitting, Experimental testing, Polyethylene foam

3. Introduction

Recent progress in material processing renewed interest in material and design optimization directed to development of novel materials with exceptional properties that cannot be found in nature. It has already been proven that materials with extreme damping can be assembled as composite materials in which it is admitted that one of the phases has a negative stiffness [1-2]. Bounds on composite elastic properties can then be applied on material properties defined in complex space (where the imaginary part stands for the loss modulus) with the help of the dynamic elastic-viscoelastic correspondence principle. Extreme damping can be achieved by further tailoring of the material data.

Besides theoretical studies, practical applications are based on composites in Reuss configurations stabilized by displacement control of the testing machine, solicited by harmonic low frequency (around 1Hz) excitation. Such a concept has been presented in [1, 3-4] as pre-strained objects in form of buckled tubes or cylinders embedded in a convenient matrix material. It was experimentally verified that buckled silicon rubber tubes in cement silicon matrix can increase the effective loss factor substantially, around 500 times, with respect to the values of the constituents. Effective loss modulus of 1.5GPa was achieved for polymer column dampers in the linear domain and about 1.62GPa in the small amplitude nonlinear domain; 200GPa were achieved in such dampers consisting of stainless steel columns. This is a significant advance because for most materials this value generally never exceeds 0.6GPa. The disadvantage of these solutions is that the extreme properties are reached in a resonance-like manner and therefore, its achievement is very sensitive to geometrical and other parameters. Also the manufacturing process is not very simple.

This paper is focused on material realization and numerical assessment of the negative stiffness phase. A typical representation of the negative stiffness mechanism is formed by two inclined springs/bars allowing for snap-through. Material realization to this effect, using a continuous material, is still a challenging task. The novel idea in this contribution has been formulated as to build the negative stiffness phase by polyethylene foam of low density (20-50kg/m³), or similar, with special cuts to create a Structure with inherent, periodically distributed, bistable elements (SIBE). Thus the material realization is proposed from a material that is easily available and cheap. There is no complicated manufacturing technique involved, desired shape and additional cuts can be introduced *e.g.* by water jet or heated blades. It was verified experimentally [5-8] that such a material exhibits a negative stiffness branch in the effective force displacement graph, that is maintained over a finite range of displacements, under a displacement control uniaxial tension test.

In order to optimize SIBE with regard to vibration damping, several geometrical parameters describing the position, size and shapes of the additional cuts have to be taken into account. The optimization can then be accomplished within a finite element model by a convenient optimization technique. With this objective a suitable material model is defined, its parameters are fitted and optimized according to experiments and finite element model capable of reproducing experimental tests is developed.

4. General Description of the Samples and Testing Equipment

Polyethylene is the most commonly used type of plastic, and is made up of ethylene monomers linked together. When the monomers are polymerized they are bonded together creating a stable thermoplastic, but different methods of polymerization yield different kinds of polyethylene, that can be divided into several categories depending on properties such as density and branching.

The polyethylene foam is a closed-cell cellular material, thus the structure is neither completely solid nor completely flexible; rather it assumes a semi-rigid structure. However, even in its semi-rigid form, polyethylene foam can have varying textures, appearing soft like urethane foams or harder like some polystyrene foams. Low-density polyethylene foam has numerous applications because of its many desirable properties including water-resistance, chemical resistance, energy-absorbance, buoyancy and cushioning characteristics. In order to incorporate in it an inherent bistable element, cuts of semi-circumferential shape were introduced by water jet. Apart from the additional cuts, SIBE does not need any special manufacturing technique. The base material is easily accessible and cheap. The sheets formed by two light polyethylene foam plates of density 20kg/m^3 glued together were provided by 100metros company (www.100metros.pt). The original sheet size was approximately $260 \times 260 \times 20\text{-}23\text{mm}$.

In order to analyse BM and SIBE behaviour, several experimental tests were conducted. First of all, prismatic BM samples were cut by heated blade and acrylic parts were glued at extremities in order to provide a region that could be securely fixed in the testing equipment (Figure 1a)). Three axes of orthotropy in BM samples are aligned with the specimen edges. Directions in plane are designated as L and T . L stands for the direction aligned with the longer axis of the bubbles that have ellipsoidal shape, *i.e.* with the stiffer direction. T designates the direction along the shorter ellipsoid axis. The third direction, across the thickness, can be assumed to have properties T . Letters L and T are therefore used for samples identification and designate the direction of solicitation in the testing machine. SIBE samples were cut by water jet in the way that the snap-through mechanism works in the stiffer L -direction; schematics in presented in Figure 1b). Acrylic parts were also glued at the edges that were fixed in the testing machine.

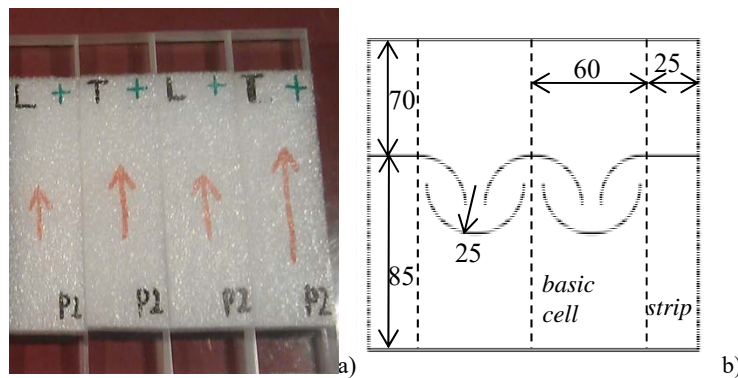


Figure 1. a) BM specimens, b) SIBE schematics – two basic cells with lateral strips (dimensions in mm)

The testing equipment at NTIS/UWB is composed of the electromechanic testing machine Zwick/Roell Z050 (Figure 2) and the four-camera 3D digital image correlation system Dantec Dynamics Q-400, GenTL/GenICam that secures the data acquisition and data analysis.

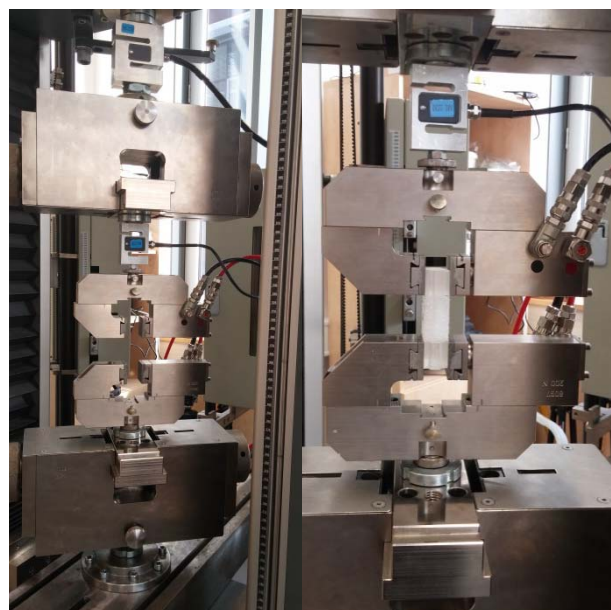


Figure 2. Electromechanic testing machine Zwick/Roell Z050

The testing equipment at IDMEC/IST is composed of the universal test machine (model 5566, Instron Corporation Canton, USA) with a load cell of 500N accompany by the digital image correlation equipment from Correlated Solutions with data acquirement by one VIC camera and VIC Snap software. The images gathered should be processed by VIC2D software.

At both institutions the digital image correlation technique was used to obtain a contour map of displacements of the entire specimen surface according to mechanical tests guided by the testing machine. The digital image correlation (DIC) is an optical method which uses a mathematical correlation analysis to examine digital image data taken while samples are in mechanical tests. The results are dependent on the digital image resolution, the width and the height of the specimen, the distance between camera and the specimen, the focal length of the lens and the application of the speckle pattern. The speckle pattern can be applied with white and black paints. All the images taken during deformation are compared with a reference image which shows the difference in this speckle pattern. Differences are calculated by correlating all the pixels of the reference image and any deformed image. This way a displacement distribution map can be created. In this work, firstly, the surface of polyethylene samples was painted with a thin layer of white acrylic paint and then a black mist of paint was applied to get the black speckles. During the tests digital camera(s) recorded the specimens and digital images were then processed by adequate software.

4. BM Tests

BM specimens were tested on testing machines at both institutions. Due to the samples forms, it can be expected that the distribution of stresses and strains over the specimens will be approximately uniform. The output from the testing machine in form of the applied force versus the imposed displacement could thus be easily transformed to nominal stress-engineering strain dependence. There are however two reasons why these results are not sufficient. The first reason is that the transversal strains are not recorded. There is a possibility to add strain gauges, but this could damage the specimen surface due to its specific microstructure. The second reason is that it was observed that glued extremities of the specimens were much more sensitive to strains, because the microstructure was affected by the cut in bubbles and altered by the chemical reaction with the glue. Therefore, the recorded strains from the testing machine were significantly larger (in absolute values) than in the body of the specimen. Due to the altered properties in the glued area and limited glue strength, this was also the part sensitive to rupture. From the “unglued” surface it was not clear enough if the rupture was caused by reaching the strength in the glue or in the cut in bubbles, but this was not important for the objectives followed.

Several tests were performed, but due to the high viscous effects, only cyclic tests were used for fitting the material properties. Four cyclic tests were accomplished together with 2D VIC equipment. Samples and tests are identified in Table 1.

Table 1. Specification of BM samples and tests used together with VIC equipment

	Width [mm]	Thickness [mm]	Length [mm]	Test 1	Test 2
BM0L	38.35	21.94	134.0	3x(4mm/-4mm) ascending 4mm/min descending 4mm/min	3x(5mm/-4mm) ascending 8mm/min descending 4mm/min
BM0T	38.55	22.39	133.4		

Unfortunately, it was not possible to reach higher levels of compression because the samples were quite long and therefore bended at higher compressive strains due to some imperfections that prevented to keep the samples in pure compression. Results of Test 1 are shown in Figure 3.

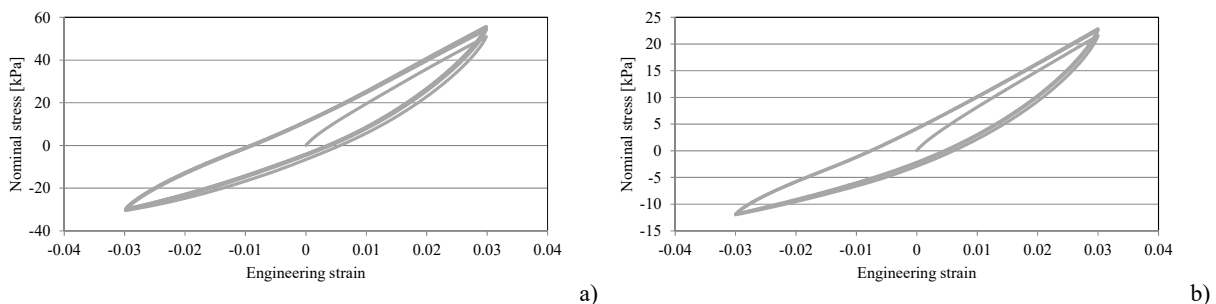


Figure 3. Test 1: a) L-direction, b) T-direction

To minimize the negative effect of bending, smaller specimens were prepared and tested at NTIS/UWB; dimensions and designations are given in Table 2. Set of tests was prepared to confirm the previous conclusions (Table 3), this time however without DIC, but estimates from the previous tests for transversal strains and reduction of longitudinal strains could be used. Also here some tests could

not be fully completed for reasons specified previously, because a rupture in high tension occurred quite often at the glued surface, (Figure 4). Summary of completed tests is given in Table 4.

Generally speaking, there was almost no difference between the test results, different strain rates only affected the first branch of the stress-strain graph of the cyclic tests, but the hysteretic loop remained practically unchanged in all tests. This is shown in Figure 5.

Table 2. Specification of BM samples tested at NTIS

	Width [mm]	Thickness [mm]	Length [mm]
BM1L	30.30	20.2	40.40
BM1T	30.29	20.2	39.40
BM2L	29.33	20.2	39.39
BM2T	31.31	20.2	39.38
BM3L	30.31	20.2	40.40
BM3T	31.31	20.2	39.39

Table 3. Specification of tests accomplished at NTIS

	8mm/min	16mm/min	32mm/min
3x(4/-4mm)+0	Test3	Test4	Test5
3x(8/-8mm)+0			Test6
3x(8/-8mm) +3x(12/-12mm)+0			Test7
3x(8/-8mm) +3x(8/-12mm)+0	Test8	Test9	



Figure 4. Failure of BM specimens in tension

Table 4. Summary of completed tests

	Test3	Test4	Test5	Test6	Test7	Test8	Test9
BM1L	OK	OK	OK	OK			
BM1T	OK	OK	OK		OK		
BM2L	OK	OK	OK	OK			
BM2T	X						
BM3L	OK	OK	OK			OK	
BM3T	OK	OK	OK			OK	OK

Tests 6-9 are omitted in Figure 5 because the tension solicitation was already affected by the failure progression. Nevertheless, the other parts of the experimental curve are in conformity with Tests 3-5 and did not bring much new.

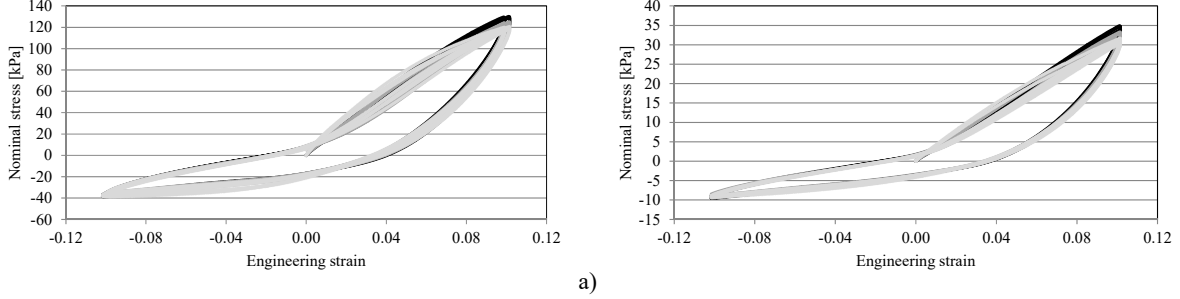


Figure 5. Test 3 on 3 specimens (light grey), Test 4 on 3 specimens (dark grey), Test 5 on 3 specimens (black): a) L-direction, b) T-direction

As can be observed from Figures 3 and 5, by rough linearization using the extreme values registered, it can be concluded that the level of orthotropy is approximately 2.5 for small strains (0.03) and around 4 for large strains (0.1). This ratio is verified for both, tension as well as compression. The ratio of moduli between tension and compression solicitation is approximately 2 for small strains (0.03) and 3.4 for large strains (0.1).

5. Understanding the Material Model

After analysing several hyperelastic formulations, the generalized Fung orthotropic foam was selected as the main material model. Viscoelasticity was added by Prony series and behaviour in tension and compression was controlled by internal state variables specified in the user defined subroutines implemented in software ABAQUS.

Before proceeding to the material fitting, analysis of the capabilities and limitations of the material model used was accomplished. For this purpose, a semi-analytical solution of the uniaxial test was derived. In fact all tests on BM can be solved this way, because it can be assumed that distributions of strains and stresses in the specimen are uniform. In uniaxial test, principal axes of strains and stresses are aligned with the specimen edges, i.e. with the directions of orthotropy, and therefore shear stresses and distortions can be omitted in the following derivation.

The generalized Fung material model is defined by the strain energy density in the form of

$$W = \frac{c}{2}(e^\varrho - 1) + \frac{1}{d} \left(\frac{J^2 - 1}{2} - \ln J \right) \quad (1)$$

The initial deviatoric elasticity tensor and the initial bulk modulus are given by

$$\bar{\mathbf{D}}_0 = c\mathbf{b} \quad \text{and} \quad K_0 = \frac{2}{d} \quad (2)$$

where c and d are model parameters with units of stress and inverse of stress, respectively. From now on, the upper bar will designate the deviatoric character. Dimensionless material data in fourth-order symmetric tensor \mathbf{b} specify the orthotropy and J is the volumetric ratio given by the determinant of the deformation gradient $J = \det(\mathbf{F})$. Further

$$\mathbf{Q} = \bar{\boldsymbol{\varepsilon}}^G : \mathbf{b} : \bar{\boldsymbol{\varepsilon}}^G \quad (3)$$

where $\bar{\boldsymbol{\varepsilon}}^G$ is the modified Green strain tensor given by $\bar{\boldsymbol{\varepsilon}}^G = (\bar{\mathbf{C}} - \mathbf{1})/2$ where $\bar{\mathbf{C}} = J^{-2/3}\mathbf{C}$, and $\mathbf{C} = \mathbf{F}^T\mathbf{F}$ is the right Cauchy-Green deformation tensor. For orthotropic material the fourth order tensor \mathbf{b} can be written in a matrix form. It is useful to analyse the matrix \mathbf{b} and its relation to the initial engineering moduli. From the term containing \mathbf{b} only deviatoric part of the stresses is taken, therefore the initial moduli from $\bar{\mathbf{D}}_0 = c\mathbf{b}$ will be the same as if the associated fully deviatoric form $\bar{\mathbf{b}}$ was used. It can be concluded that

$$E_L = \frac{9cK_0}{4K_0 + c}, \quad E_T = \frac{9cK_0(4\bar{b}_{22} - 1)}{c(4\bar{b}_{22} - 1) + 4K_0(\bar{b}_{22} + 2)}, \quad \nu_{LT} = \frac{2K_0 - c}{4K_0 + c} \quad (4)$$

These simple formulas can be used to estimate the initial values in optimization algorithm, according to predicted Young's moduli and Poisson's ratios of rough linearization of experimental results. Essentially, \bar{b}_{22} is controlling the level of orthotropy, c the slope in stress-strain graphs and d the compressibility governed by the Poisson ratios. Differences in behaviour between cases where the original \mathbf{b} and the related fully deviatoric matrix $\bar{\mathbf{b}}$ are used, are only noticeable at larger strains. Nevertheless, the fully deviatoric matrix can be used in the semi-analytical procedure, but not in the finite element code ABAQUS. Due to numerical reasons, it is necessary to use matrices that are positive definite.

Considering the two-dimensional case, the option of plane strain has to be chosen, unless ABAQUS ignores compressibility. Then \bar{b}_{12} does not have to be equal to $-1/2$. Starting in this case with the reduced stiffness deviatoric matrix, the following formulas can be obtained

$$E_L = \frac{c(\bar{c}b_{22} + K_0(1 + \bar{b}_{22} - 2\bar{b}_{12}) - \bar{b}_{12}^2 c)}{K_0 + c\bar{b}_{22}}, \quad E_T = \frac{c(\bar{c}b_{22} + K_0(1 + \bar{b}_{22} - 2\bar{b}_{12}) - \bar{b}_{12}^2 c)}{K_0 + c} \quad (5)$$

which unfortunately does not allow defining the desirable level of orthotropy, unless it is admitted that the bulk modulus can have very low values.

Viscoelastic effects are added by Prony series. Because there are no temperature effects considered and moduli ratios in the Prony series expansion of the relaxation moduli are considered the same for the deviatoric and volumetric parts, the basic hereditary (convolution) integral can be applied directly on the Cauchy stress that can be separated into the instantaneous and viscous parts. In the BM tests there is only one stress component to be considered, in the direction of the load. This semi-analytical approach greatly simplified the material fitting of BM experiments, when the stress and strain distribution is assumed uniform over the specimen and all calculation can be done in principal coordinates that coincides with the axes of orthotropy. Moreover, the numerical ABAQUS results were sometimes doubtful, especially in the case of very tight creep tolerance and fine time step. In fact, these parameters should increase the numerical precision, but the opposite was verified. Therefore options in numerical calculations were confirmed by the semi-analytical results.

6. BM Material Fitting – Small Strains

First of all, material fitting was carried out on BM Test 1 from Table 1. Matlab programs were written to manipulate and visualize VIC data. It was concluded that due to the non-smooth surface sensible to reflections some results can be distorted. In addition, due to the material structure inherent to closed cell foams and non-homogeneity at microscale, developed strains are locally non-uniform across the bubbles. Therefore, strain distribution from VIC data is not convenient for further usage due to large oscillations. Consequently, displacement fields were used for strain calculation. The programs written in Matlab have possibility to disregard some rows and/or lines from the data table close to the edges, where the results are less reliable. In addition, results are tested against a given percentile and unsuitable data are removed. Final set of data is interpolated by bilinear function and slopes are used to define the corresponding engineering strains, and consequently stretches and logarithmic strains. With these data it is also possible to recalculate the force recorded by the testing machine to true Cauchy stress.

Due to the large orthotropy, material fitting was programed for two directions of orthotropy simultaneously, and for the sake of simplicity, on one element unit cube. At each optimization loop this cube was subjected to two tests in different directions. These tests were displacement-controlled in conformity with the experiments. In each test, strain in testing direction was prescribed as a function of time, and stress in testing direction and strain in transverse to testing direction were extracted. Thus four-array entries were used in curve fitting Matlab algorithm. Optimization module was programmed in Matlab with automatic connection to ABAQUS calculation and results extraction. To improve fitting performance, initial guess of material data was done using the semi-analytical results of the generalized Fung model described in the previous section. In order to capture different behaviour in tension and in compression, stepped and ramped evolution of material parameters was implemented according to the developed strain with the help of user defined subroutines. Results of fitting are plotted in Figures 6 and 7. Stepped variation of material data had slightly lower least square norm, but, generally speaking, ramped variation of material properties performed better, as can be observed in the figures.

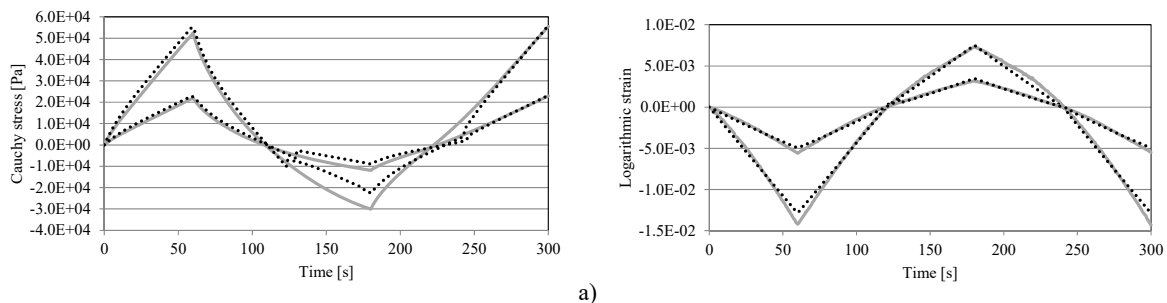


Figure 6. Fitting of experimental data with stepped variation of material properties: a) stresses, b) strains (experiment-grey lines, fitted results-black dotted lines)

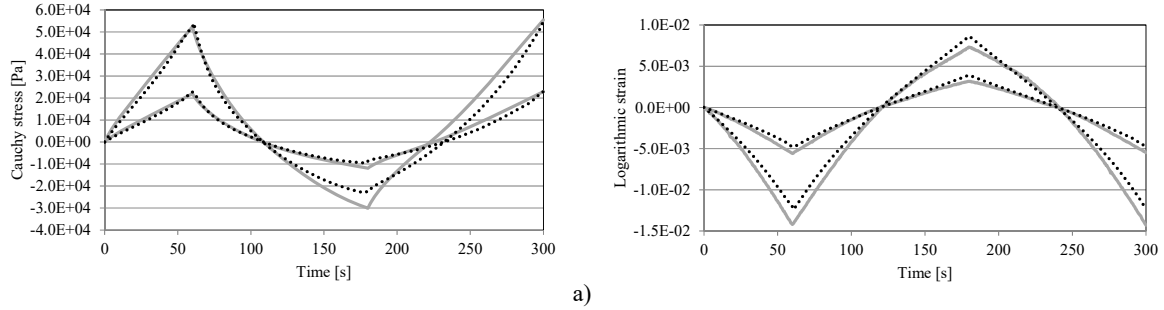


Figure 7. Fitting of experimental data with ramped variation of material properties: a) stresses, b) strains (experiment-grey lines, fitted results-black dotted lines)

Final results are summarized in Table 5 for the ramped option. For numerical stability fully deviatoric matrix $\bar{\mathbf{b}}$ could not be used, therefore each term in it was increased by 0.1.

Table 5. Material parameters obtained by fitting the experimental results of Test 1 (ramped option)

Ramped	c [MPa]	d [Pa^{-1}]	b_{22}
Tension	0.777	1.54E-08	0.61
Compression	0.361	3.15E-06	0.58

Regarding the viscoelasticity, only one term of Prony series was used. Fitting with regard to these parameters was quite stable, giving the relative moduli of 0.5 and relaxation time of 10s.

6. BM Material Fitting – Large Strains

Next, material fitting was carried out on BM Tests 3-5 from Table 3. Because all these tests involve quite large strains, numerical results calculated in software ABAQUS were additionally checked by the semi-analytical solution. First of all, the semi-analytical procedure without viscoelastic effects was used to fit approximately the extreme values. Results of such fitting are plotted in Figure 8, where for the sake of clarity only averaged results of Test 3 are included. The corresponding material parameters are summarized in Table 6. In this case the matrix $\bar{\mathbf{b}}$ was fully deviatoric. It is seen that, with respect to Table 5, stiffness c -values are significantly lower, because the effect of viscoelastic moduli is omitted. The ratio of c -values in tension and compression is higher, because the softening tendency in compression is more pronounced in larger strains. In this fitting b_{22} -value was kept fixed. The strategy was different; four target extreme values were defined, thus there were four parameters to be determined and exact solution was reached. This solution was independent on the initial stage. Nevertheless, as viscous effects were neglected, further investigation had to be carried on.

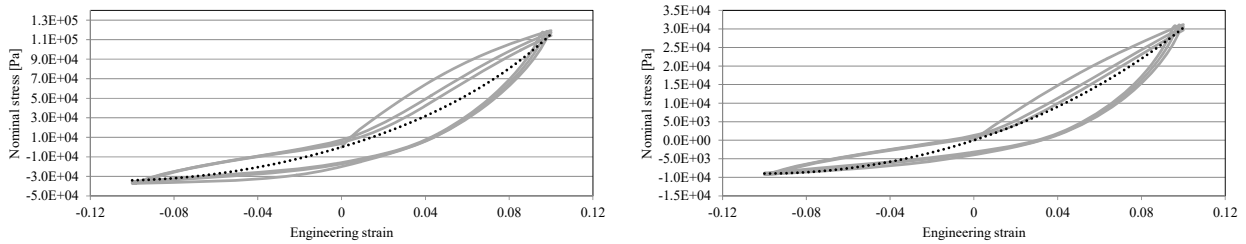


Figure 8. Fitting of experimental data with ramped variation of material properties: hysteretic loop in L-direction (left), hysteretic loop in T-direction (right); (experiment-grey lines, fitted results-black dotted lines)

Table 6. Material parameters obtained by Matlab procedure by fitting Tests 3-5 (viscoelasticity omitted)

Ramped	c [MPa]	d [Pa^{-1}]	b_{22}
Tension	0.56	2.0E-06	0.39
Compression	0.19	11.2E-06	0.39

After several alternative strategies, best results were obtained by the semi-analytical procedure described in previous sections, as shown in Figure 9. Material parameters from this analysis are given in Table 7. This time viscoelastic data were 0.6 and 10s. It is seen that better results for large strains would probably be obtained with two terms in Prony series.

Table 7. Material parameters obtained by semi-analytical procedure by fitting Tests 3-5 (viscoelasticity included)

Ramped	c [MPa]	d [Pa^{-1}]	b_{22}
Tension	0.31	$4\text{E-}07$	0.39
Compression	0.12	$1\text{E-}05$	0.39

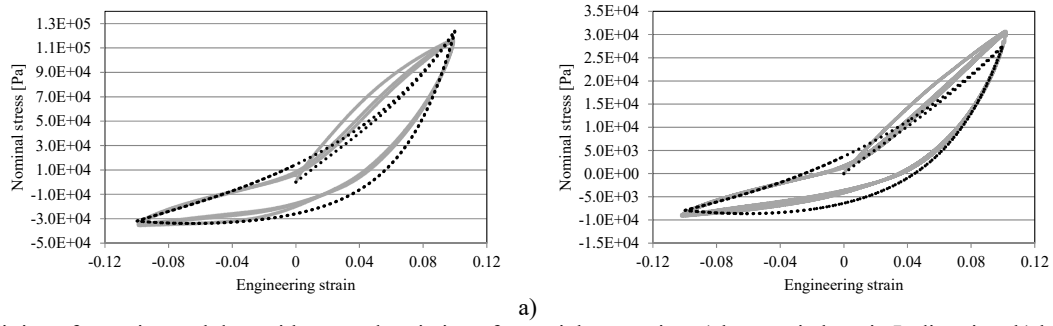


Figure 9. Fitting of experimental data with ramped variation of material properties: a) hysteresis loop in L-direction, b) hysteresis loop in T-direction (experiment-grey lines, fitted results-black dotted lines)

7. SIBE Experimental Tests

Tests on SIBE specimens were accomplished on testing machines at both institutions and complemented by DIC technique. For tests accompanying by DIC technique, the surface of the specimen was covered by speckle pattern, as shown in Figure 10.

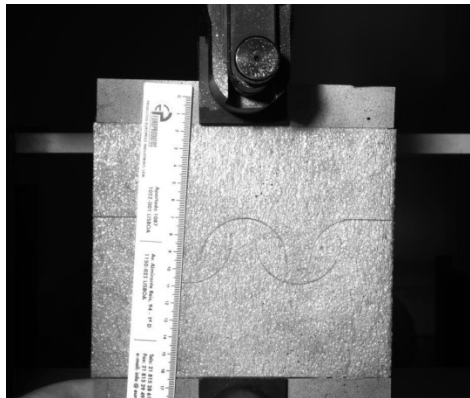
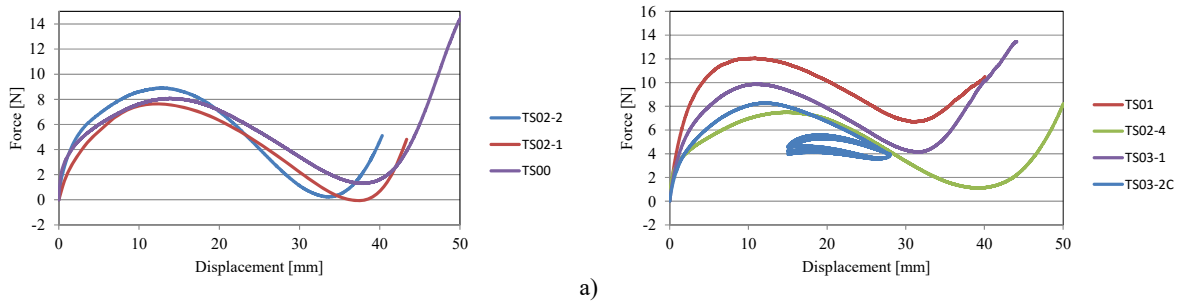


Figure 10. SIBE test: sample covered by the speckle pattern

Force-displacement graphs from the testing machines are summarized in Figure 11. It is seen that there can be significant differences between specimens, but a particular specimen usually have very similar force-displacement evolution.



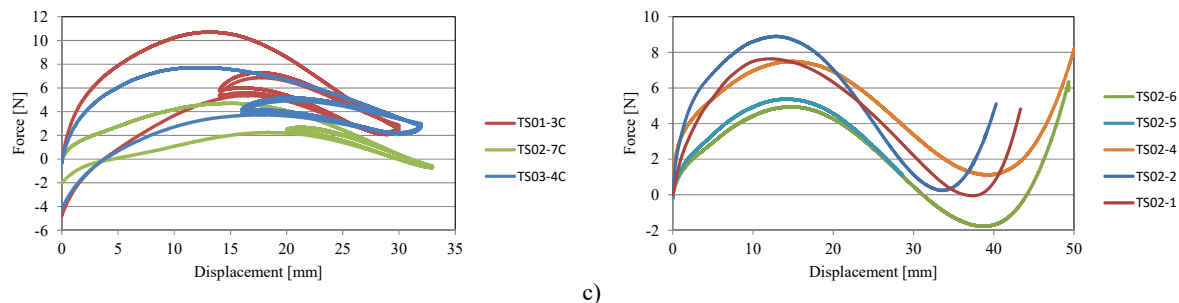


Figure 11. Force-displacement graphs from the testing machines: a) initial tests without DIC, b) new tests from IDMEC/IST with DIC, c) new tests from NTIS/UWB with DIC, d) summary of all tests performed at the same specimen

The differences are caused by slight discrepancies in lengths of the additional cuts and other imperfections, that may cause that the specimen suffer from significant out-of-plane deformations and then usually higher force is necessary to initiate the snap-through mechanism. Regarding the hysteric loop, it performs in the opposite slope as it was intended, but the first loop significantly loses its initial slope. Nevertheless, then the other loops are quite stable and follow the first loop.

8. Conclusion

In this paper the polyethylene foam sheets were utilized as a base material for a structure exhibiting a negative stiffness over a finite range of global strains provided by inherent bistable elements. Convenient material model was identified, and several optimization strategies were proposed for its material parameters fitting based on results obtained from experiments. Optimization modules were written in Matlab environment, connected with ABAQUS software or Maple calculations based on semi-analytical developments. Then a finite element model capable of reproducing experimental tests was developed.

9. Acknowledgements

Jan Heczko and Libor Lobovský were supported by the project LO1506 of the Czech Ministry of Education, Youth and Sports. The work developed by the first author was sponsored by SFRH/BSAB/113776 attributed by Fundação para a Ciência e a Tecnologia in Portugal. In addition, project UID/EMS/50022/2013 is appreciated.

10. References

1. Lakes R.S. 2001. Extreme damping in compliant composites with a negative-stiffness phase, *Philosophical Magazine Letters*, 81(2), 95–100.
2. Jaglinski T., Kochmann D., Stone D. and Lakes R.S. 2007. Materials with Viscoelastic Stiffness Greater than Diamond. *Science* 315(Feb.): 620-622.
3. Kalathur H. and Lakes R.S. 2013. Column Dampers with Negative Stiffness: High Damping at Small Amplitude. *Smart Materials and Structures* 22(8): 084013-21.
4. Dong L. and Lakes R.S. 2013. Advanced damper with high stiffness and high hysteresis damping based on negative structural stiffness, *International Journal of Solids and Structures*, 50(14–15), 2416–2423.
5. Heczko J., Dimitrovová Z. and Rodrigues H.C. 2013. Composite material with negative stiffness inclusion for vibration damping: The effect of a nonlinear bistable element. In Z. Dimitrovová, JR. de Almeida & R. Gonçalves (eds) *Proc. 11th International Conference on Vibration Problems (ICOVP-2013)*, Lisbon, Portugal, 9-12 September.
6. Heczko J., Dimitrovová Z. and Rodrigues H.C. 2014a. Negative stiffness materials for vibration damping: a material realization of a nonlinear bistable element. *International Journal of Innovations in Materials Science and Engineering* 1(2): 75-81.
7. Heczko J., Dimitrovová Z. and Rodrigues H.C. 2014b. “Optimization of a material with a negative stiffness provided by an inherent bistable element”, in A. Araújo (editor), *Engineering Optimization 2014*, CRC Press 2014. *Proc. 4th International Conference on Engineering Optimization (EngOpt 2014)*, Lisboa, Portugal, 8 -11 September.
8. Dimitrovová Z., Heczko J. and Rodrigues H.C. 2015. “Structural optimization of a material exhibiting negative stiffness”, *Proc. IFToMM International Conference on Engineering Vibration (ICoEV-2015)*, Ljubljana, Slovenia, 7-10 September.